Teng et al. Nanoscale Research Letters (2015) 10:384
DOI 10.1186/s11671-015-1088-8

Nanoscale Research Letters
a SpringerOpen Journal

NANO EXPRESS Open Access

Fabrication and Characterization of Monodisperse Magnetic Porous Nickel Microspheres as Novel Catalysts

Chao Teng, Jie He, Lili Zhu, Lianbing Ren, Jiwei Chen, Mei Hong* and Yong Wang*

Abstract

A facile and efficient hard-templating strategy is reported for the preparation of porous nickel microspheres with excellent uniformity and strong magnetism. The strategy involves impregnation of porous polymer microspheres with nickel precursors, calcination to remove the template, followed by thermal reduction. The morphology, structure, and the property of the Ni microspheres were characterized by scanning electron microscopy, X-ray powder diffraction, N_2 adsorption-desorption isotherms, thermogravimetric analysis, and magnetic hysteresis measurement. The obtained porous nickel microspheres were monodispersed with a particle size of 0.91 μm and crystallite size of 52 nm. Their saturation magnetization was much higher than that of Ni nanoparticles. The unique porous nanostructured Ni microspheres possess catalytic activity and excellent recyclability, as demonstrated in the catalytic reduction of 4-nitrophenol to 4-aminophenol. The microperical Ni catalysts could be easily separated either by an external magnetic field or by simple filtration.

Keywords: Magnetic microspheres; Porous nickel microspheres; Separable catalysts

PACS: 61.46.Hk; 75.75.-c; 81.07.-b

Background

The development of nanoscience and nanotechnology has put forward a higher requirement to fabricate novel nanostructured catalysts with specific morphologies and functions [1–9]. A broad range of nanostructured metals such as Au, Ag, Fe, Cu, Pt, Pd, and Ni have shown enhanced catalytic properties for applications in organic synthesis [10–12]. Among different morphologies of metals, hierarchically porous spheres have attracted great research interests. Several reports demonstrated that assembling metal nanoparticles into porous hierarchical spheres led to improved properties over multiple-length scales [13–17]. Microspheres possess higher flowability and would not tend to agglomerate, which is inevitable for their nanoparticle counterparts. They also showed high catalytic efficiency derived from a high surface-to-volume ratio and maximized transport efficiency [18–22].

Porous nickel (Ni) catalysts have long been successfully employed in hydrogenation reactions, chemoselective oxidative coupling of thiols, and Hantzsch condensation etc. [23–27]. Another important feature of Ni catalysts is their ferromagnetic properties. This offers possibility to easily remove the spent catalysts by magnetic field for the next reaction cycle.

The intrinsic properties of the Ni catalysts, such as catalytic activity and distinctive magnetic property, are deeply affected by their size, crystallinity, composition, and morphology [28–32]. Extensive efforts [33–40] have been devoted to fabricate various structures of porous Ni catalysts, making use of template synthesis, self-assembly, electro/chemical bath deposition, sol-gel method, and so on. The traditional RANEY® Ni, one of the most widely used Ni catalysts in industry, is prepared by chemical leaching and consists essentially of a porous skeletal structure exhibiting high catalytic activity. However, the fine powder nature of RANEY® Ni results in difficult catalyst separation from liquid phase reactions or plugging and pressure build-up in the fixed bed systems [41–45]. Recently, Fow's group [46–48] prepared gauze-supported

* Correspondence: hongmei@pkusz.edu.cn; ywang@pkusz.edu.cn
Guangdong Provincial Key Laboratory of Nano-Micro Materials Research, School of Chemical Biology & Biotechnology, Peking University Shenzhen Graduate School, Shenzhen 518055, China

skeletal Ni catalysts which may be adapted to various reactor configurations by folding or stacking. However, supported catalysts are quite complex, and their fabrication approaches are time-consuming. For free standing Ni catalysts, Wu's group [49] demonstrated a facile template- and surfactant-free method to prepare porous hierarchical Ni nanostructures by directly calcining the Ni-based flower-like precursor in Ar. Zhu et al. [50] developed a novel precursor hydrothermal redox method to fabricate the hierarchically porous structure of Ni hollow microspheres consisting of Ni nanoparticles on the shell. Yuan et al. [40] self-assembled synthesized porous Ni phosphate/phosphonate hybrid microspheres to combine the merits of organic and inorganic components. The hybrids showed catalytic activity for the reduction of 4-nitrophenol (4-NP) to 4-aminophenol (4-AP) due to the presence of Ni active sites on the pore surface. However, the Ni nanostructures produced from these soft-templating or template-free approaches were typically not uniform due to the undirected nucleation sites in the homogenous system.

In our previous works, we developed a hard-templating method utilizing monodisperse polymer microspheres to prepare uniform porous inorganic microspheres consisting of metal or metal oxide nanoparticles [51–54]. In this report, we applied the same principle to fabricate monodisperse porous Ni oxide microspheres by impregnation of porous polymer microspheres with Ni precursors followed by calcination to remove the template. Subsequent thermal reduction led to Ni microspheres. Different analysis techniques, such as scanning electron microscopy (SEM), X-ray powder diffraction, N_2 adsorption-desorption isotherms, and magnetization curves were adopted to characterize the size, morphology, and magnetic property of the obtained microspheres. Their catalytic properties were also primarily studied.

Methods

Materials

The Ni precursor nickel acetate ($Ni(Ac)_2 \cdot 4H_2O$) was purchased from Alfa Aesar. Ethylenediamine (EDA) was purchased from Sigma-Aldrich. The hard template porous polymer microsphere named poly(GMA-co-EGDMA) is a polymer of glycidyl methacrylate (GMA) cross-linked with ethylene glycol dimethacrylate (EGDMA) supplied by Nano-Micro Technology Company, China. 4-NP and $NaBH_4$ used in the catalytic study of porous Ni microspheres were purchased from Sigma-Aldrich. Water was purified by distillation followed by deionization using ion exchange resins. Other chemicals were analytical grade and used without further purification.

Preparation of Porous Nickel Oxide (NiO) and Ni Microspheres

Monodisperse porous NiO microspheres were fabricated by impregnation of porous poly(GMA-co-EGDMA) microspheres with Ni precursors followed by calcination to remove the template. In a typical synthesis, the poly(GMA-co-EGDMA) microspheres were firstly functionalized by EDA following our previous protocol [51]. Poly(GMA-co-EGDMA) microspheres of 10 g were dispersed in 240 ml water and sonicated for 0.5 h before 10 g of EDA was added, and the mixture was mechanically stirred at 80 °C for 13 h. The resulting EDA-functionalized poly(GMA-co-EGDMA) microspheres were washed repeatedly with distilled water till the filtrate was neutral, and the filter cake was dried at 50 °C. Afterwards, the EDA-functionalized poly(GMA-co-EGDMA) microspheres of 1 g were mixed with 0.5 g of $Ni(Ac)_2 \cdot 4H_2O$, 6 ml of ethanol, and 4 ml of water. The mixture was then sonicated for 10 min and dried at 90 °C. Finally, the obtained composite microspheres were calcined at 600 °C for 12 h to form monodisperse porous NiO microspheres, which were subsequently reduced in a 95 % N_2 / 5 % H_2 atmosphere at 500 °C for 10 h to form porous Ni microspheres.

Catalytic Study of Porous Ni Microspheres

The reduction of 4-NP by $NaBH_4$ was chosen as a model reaction for investigating the catalytic performance of porous Ni microspheres. In a typical reaction, aqueous solution of 4-NP (5 mM, 1 ml) was mixed with fresh aqueous solution of $NaBH_4$ (0.1 M, 5 ml) at room temperature. The microspheres (1.0 mg) were rapidly added into the reaction system. Subsequently, 1 ml of aqueous suspension was sampled at a given interval and filtered through a 0.45-μm membrane. The UV-visible absorption spectra of the filtrates were recorded at room temperature to monitor the reaction progress.

Characterizations

Powder X-ray diffraction (XRD) of the synthesized microspheres was recorded using a Rigaku D/Max-2200PC diffractometer with Cu Kα at 40 KV, 200 mA. The crystallite size of the microspheres determined by XRD was calculated by the Williamson-Hall method. A field emission scanning electron microscope (SEM) Hitachi S4800 was used for the determination of the morphology and structure of the microspheres. The particle size of the microspheres was measured by a Beckman Coulter Counter size analyzer Multisizer 3. N_2 adsorption-desorption isotherms were performed at 77 K on a Micromeritics Tristar 3020. The magnetic measurement of porous Ni microspheres was carried out at room temperature

with a vibrating sample magnetometer under a varying magnetic field (ISOM, UPM, Madrid, Spain).

Results and Discussion

Preparation and Characterization of Porous Ni Microspheres

In our previous work, monodisperse porous silica, magnetic nanoparticle-embedded silica microspheres, carbon microspheres, and zirconia microspheres have been successfully prepared using porous polymer microspheres as the hard template [51–55]. Notably, the unique pore structure and well-defined morphology of the parent polymer microspheres were inversely replicated into the obtained inorganic microspheres with similar monodispersity, which led to desired properties. This promising hard-templating method, as shown in Scheme 1, was used in this work to fabricate porous Ni microspheres. Porous poly(GMA-co-EGDMA) microspheres were chosen as the parent because of their easy functionalization due to the existence of surface epoxy groups. Functionalization by EDA introduced amino group to the porous poly(GMA-co-EGDMA) microspheres, which aided the impregnation of Ni precursor $Ni(Ac)_2 \cdot 4H_2O$ into the pore space. During the impregnation and drying process, the Ni precursors penetrated into the pores and incorporated into polymer microspheres to form composite microspheres. Calcination at 600 °C removed the polymer template, and at the same time oxidized the Ni precursor to NiO microspheres. Afterwards, the porous NiO microspheres were reduced in a hydrogen atmosphere to form porous Ni microspheres. Attempts to directly decompose the polymer in the Ni composite microspheres in a reducing hydrogen atmosphere to avert the step of forming NiO failed as the spherical structure collapsed due to the huge property differences between the polymer template and Ni.

SEM images displayed in Fig. 1 demonstrate that the structured three-dimensional network of the parent polymer microspheres was well preserved in the synthesized porous NiO microspheres and porous Ni microspheres. Therefore, Ni precursors entered into the pores and interacted closely with the polymer skeleton. After reduction, the obtained porous Ni microspheres kept excellent monodispersity and well-defined spherical morphology. Due to the crystallite transformation at high temperature during reduction, the nanoparticles in Ni microspheres are larger than that of the NiO microspheres. As seen from the particle size of the polymer template and the synthesized microspheres in Table 1, the composite microspheres show similar size and monodispersity to the original polymer microspheres indicating that Ni precursor penetration did not cause structure deformation. Compared with the template microspheres (Fig. 1a–c), the porous NiO microspheres (Fig. 1d–f) were smaller probably due to shrinkage of the skeleton, high density of NiO, and growth of NiO crystallite size during calcination. High-temperature reduction further reduced the size of the formed Ni metal microspheres (Fig. 1g–i). All these as-prepared microspheres are in excellent independent spherical morphology. Agglomeration for the Ni microspheres, typically observed for molecular self-assembled ones (Zhu et al., solid state sciences 2011;12:438–43), was not observed in our study. This demonstrated the strong templating power of our hard polymer microspheres, which counteract the surface chain-forming force caused by the magneto-static energy of ferromagnetic particles. The size distribution analyzed by the size analyzer confirmed the SEM observations (Table 1). The size of the original polymer microspheres and the polymer composite

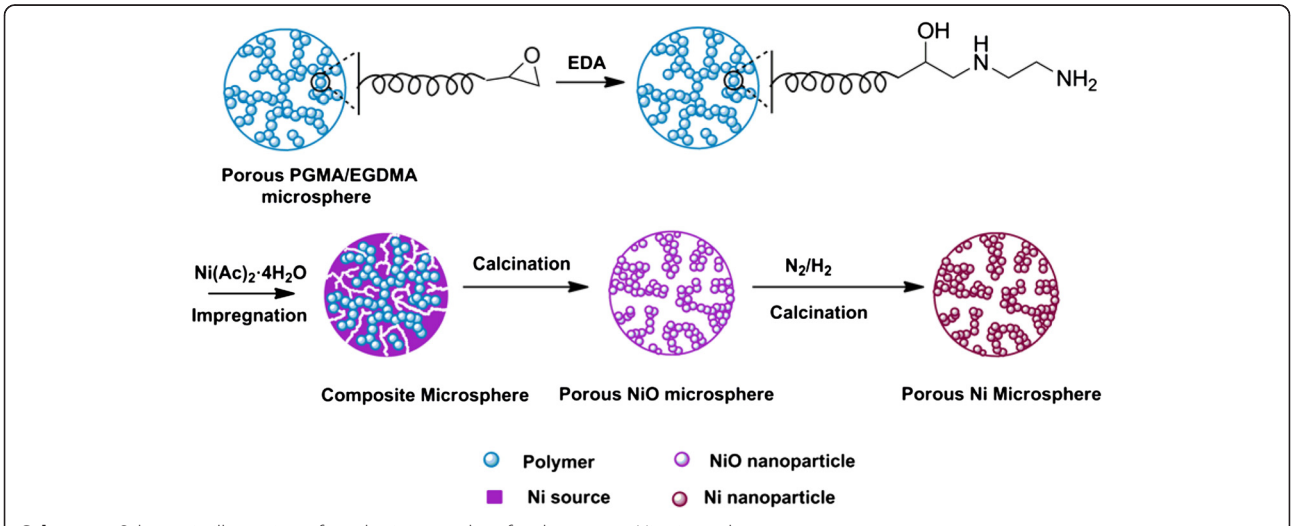

Scheme 1 Schematic illustration of synthetic procedure for the porous Ni microspheres

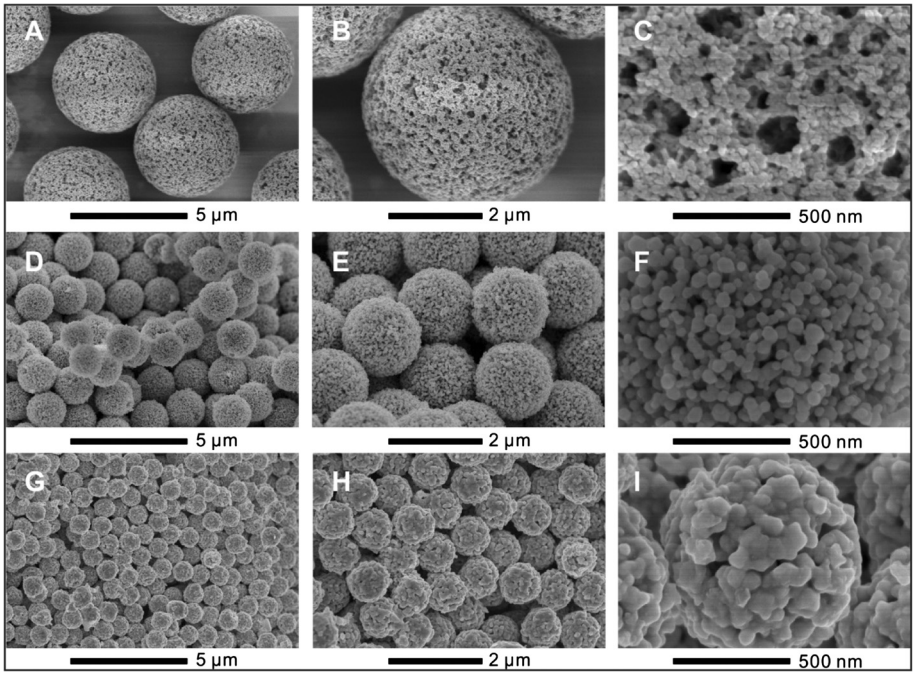

Fig. 1 SEM images of (**a**–**c**) polymer microspheres, (**d**–**f**) NiO microspheres, and (**g**–**i**) Ni microspheres under different magnification

was very close, of 4.44 and 4.49 μm, respectively. Burning out the polymer template decreased the NiO microspheres to an average size of 1.83 μm, and further reductive process reduced the Ni microspheres to 0.91 μm. All microspheres were exceptionally uniform, and the coefficient of variation for particle size of NiO and Ni metal microspheres was 4.9 and 7.7 %, respectively.

The crystalline phases and the crystallite sizes of the powders were confirmed by XRD measurements. Powder X-ray diffraction patterns revealed that the obtained porous NiO microspheres and Ni microspheres are all crystalline. The reflection peaks of NiO microspheres (shown in Fig. 2), indexed to (111), (200), (220), (311), and (222), can be well-assigned to the cubic phase of NiO (JCPDS card no. 47–1049). The average crystallite size of porous NiO microspheres, calculated based on the Williamson-Hall method, was ca. 29 nm, consistent with the SEM observation (Fig. 1f). Reduction of porous NiO microspheres at 300 °C converted most of the microspheres into Ni as the diffraction peaks of the face-centered cubic (*fcc*) phase of crystalline Ni (JCPDS card no. 04–0850) with 2θ of 44.4°, 51.7°, 76.3°, corresponding to (111), (200), and (220) planes of crystalline Ni, becoming highly intense. However, the NiO peaks were still present. Increasing the reduction temperature to 400 °C reduced the impurity amount of NiO, and only with a reduction temperature of

Table 1 Properties of template and as-prepared microspheres[a]

Microspheres	Particle size (mean + SD) (μm)	Surface area (m^2/g)	Pore size (nm)
Polymer	4.44 ± 0.11	75.33	21
Polymer/Ni	4.49 ± 0.11	58.26	21
NiO	1.83 ± 0.09	13.74	34
Ni	0.91 ± 0.07	2.55	42

[a]Particle sizes were determined by Coulter counter for polymer, polymer/Ni and NiO microspheres, and SEM for Ni microspheres; surface areas were determined using the Barrett-Emmett-Teller (BET) method, and average pore sizes were calculated using the Barrett-Joyner-Halenda (BJH) method

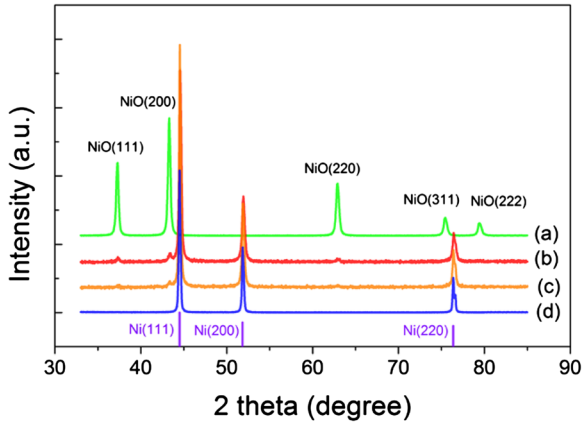

Fig. 2 Wide-angle powder XRD patterns of porous NiO microspheres and Ni microspheres reduced at 300 °C, 400 °C, and 500 °C. The *violet lines* show the standard diffractions of Ni (JCPDS No. 04–0850)

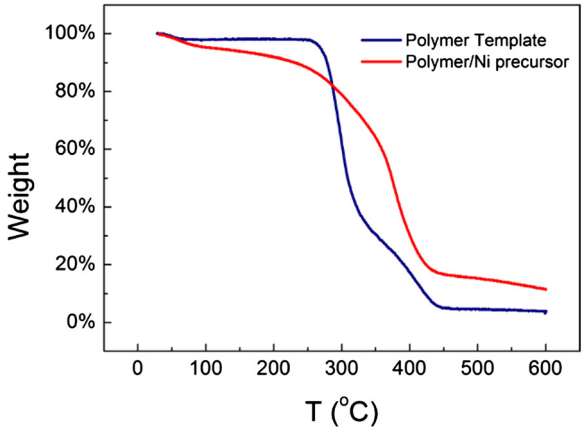

Fig. 3 TGA curve of the polymer template and polymer/Ni precursor composite microspheres

500 °C, no NiO could be seen. The crystallite size of pure Ni microspheres was calculated to be ca. 52 nm according to the Williamson-Hall method, larger than that of the NiO microspheres. Obviously, high-temperature reduction gave rise to extensive sintering due to surface condensation. The sintering behavior could also be seen in the SEM images. Although reduction at 500 °C was essential for converting NiO to Ni thoroughly, this high thermal reduction temperature created a slightly higher degree of crystallite growth and more bicontinous interpenetration of the metallic particles. Fortunately, the Ni microspheres were still separated showing smooth surfaces and clearly discernable spherical interfaces.

The nitrogen adsorption-desorption results of the microspheres are presented in Table 1, and an additional file shows the curves of N_2 adsorption-desorption isotherms and pore size distributions in more detail [see Additional file 1]. The template microspheres have a specific surface area of 75 $m^2 \cdot g^{-1}$ and pore volume of 0.38 $cm^3 \cdot g^{-1}$ with a BJH pore size of 21 nm. The composite microspheres exhibited a lower surface area of 58 $m^2 \cdot g^{-1}$ indicating that Ni precursors successfully occupied the pore voids of the polymer microspheres. After calcination, the polymer part of the composite microspheres was removed. The complete removal of the polymer template was confirmed by thermogravimetric analysis (TGA) of the composite microspheres (Fig. 3). The polymer/Ni precursor composite microspheres underwent three stages of weight loss, 25–250, 250–450, and 450–600 °C. The weight loss of 11.8 % below 250 °C could be ascribed to the gasification of small molecules such as adsorbed water and ethanol. Between 250 and 450 °C, the decomposition of polymer chain, decomposition/dehydration of nickel acetate, and crystallite formation in the composite microspheres led to a weight loss of 71.4 %, obviously lower than the 92.7 % of template polymer microspheres, due to the remaining of NiO species. Little weight loss (2.8 wt %) was observed for calcination above 450 to 600 °C. Therefore, calcination at 600 °C could assure thorough burning away of the polymer skeleton.

Porous NiO microspheres containing both mesopores and macropores were obtained with a specific surface area of 14 $m^2 \cdot g^{-1}$ and a pore volume of 0.1 $cm^3 \cdot g^{-1}$. The lower surface area and pore volume of porous NiO microspheres compared to the template microspheres were probably due to the shrinkage of the skeleton and the concurrent growth of NiO crystallites during calcination, as well as the higher density of NiO. Thermal reduction process further reduced the as-synthesized porous Ni microspheres. The Ni microspheres obtained by 500 °C thermal reduction possessed a specific surface area of 2.6 $m^2 \cdot g^{-1}$ and a pore volume of 0.01 $cm^3 \cdot g^{-1}$ with BJH mesopores of 42 nm. In contrast to porous NiO microspheres, porous Ni microspheres showed lower surface area and pore volume but larger pore size owing to phase transformation upon high-temperature reduction. To confirm the magnetic property of porous Ni microspheres, its hysteresis curve was measured at room temperature and displayed in Fig. 4. The saturation magnetization (*Ms*),

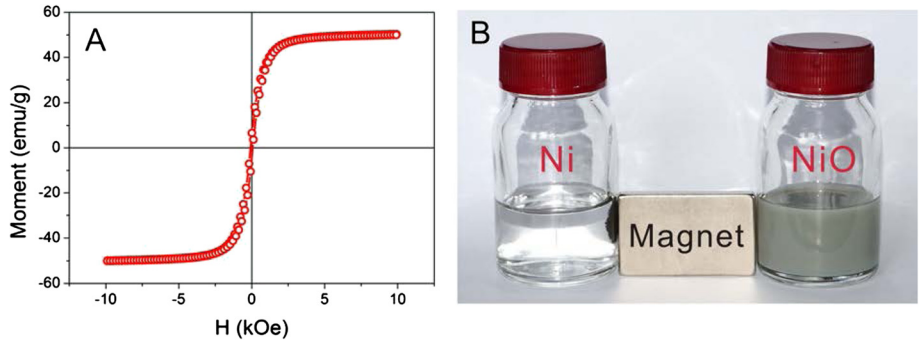

Fig. 4 a Magnetic hysteresis curves of the porous Ni microspheres. **b** Photograph of microspheres before (NiO) and after (Ni) reduction under an external magnetic field within 10 s

remnant magnetization (*Mr*), and coercivity (H_c) were measured to be 50.26 emu · g^{-1}, 4.58 emu · g^{-1}, and 65 Oe, respectively, indicating the excellent magnetic property of porous Ni microspheres, as shown in Table 2 in comparison with other reported Ni nanostructures. The Ni microspheres prepared in this work exhibited much enhanced saturation magnetization than other reported Ni nanoparticles, suggesting better resistance to surface oxidation which are known to decrease the effective magnetic moment of Ni. The saturation magnetization of Ni microspheres is very close to that of bulk Ni, and the coercivity (H_c) value is much lower, probably resulting from the shape anisotropy.

Catalytic Reduction of 4-NP by Porous Ni Microspheres

As one of the most common pollutants, 4-NP has attracted widespread attention. Many noble metal catalysts were devoted to catalyze the hydrogenation of 4-NP to obtain 4-AP which is a valuable intermediate for manufacturing anticorrosion drugs, antipyretic drugs, and analgesic. Herein, the catalytic performance of the fabricated monodisperse porous Ni microspheres for the hydrogenation of 4-NP was investigated. The reaction process was monitored by UV–vis absorbance at 400 nm.

After addition of $NaBH_4$ to the 4-NP solution, UV–vis absorbance changed from 317 to 400 nm due to the formation of 4-NPate. If no porous Ni catalyst was added, the absorbance at 400 nm remain unchanged revealing no reduction of 4-NP. When our porous Ni microspheres were added, the absorbance at 400 nm gradually decreased until no absorbance after 6 h, indicating complete reduction of 4-NP (Fig. 5). The initial bright yellow solution became colorless during the reaction course. The Ni microspheres can be easily recovered with a sand-core filter. When applying an external magnetic field, the Ni microspheres promptly transported to the wall of the reaction flask (Fig. 4), and the solution became transparent and easily separable.

Conclusions

Uniform porous NiO and Ni microspheres were fabricated by employing porous polymer microspheres as the hard template. Both NiO and Ni microspheres exhibited well-defined morphology, excellent monodispersity, mesoporosity, and high crystallinity. Calcination to remove the polymer template for NiO microspheres and thermal reduction to produce Ni microspheres grew their crystallite sizes to 29 and 52 nm, respectively. The spherical particles were instilled in the micro-size range and no inter-particle agglomeration was observed. The Ni microspheres displayed outstanding magnetism with coercivity of 64.99 Oe, saturation magnetization of 50.26 emu · g^{-1}, and remnant magnetization 4.58 emu · g^{-1}, which are superior to other Ni nanoparticles. The Ni microspheres were catalytically active in the reduction of 4-NP, and the unique morphology and strong magnetism ensured convenient separation from the reaction mixture either by simple filtration or with an external magnetic field. The general strategy presented here holds potential to be applied to the design and fabrication of more metal or metal oxide materials with better physical or chemical properties for various applications.

Table 2 Magnetism properties of Ni microspheres prepared in this study in comparison to other Ni structures

Sample	*Ms*/emu.g^{-1}	*Mr*/emu.g^{-1}	*Hc*/Oe	*Size*/nm
Ni microspheres	50.26	4.58	64.99	910 nm
Hollow Ni NPs [56]	21.1	0.69	32.3	300~450 nm
Ni nanoparticles [57]	32	5.0	40	12 nm
Bulk Ni [58]	55	2.7	100	–

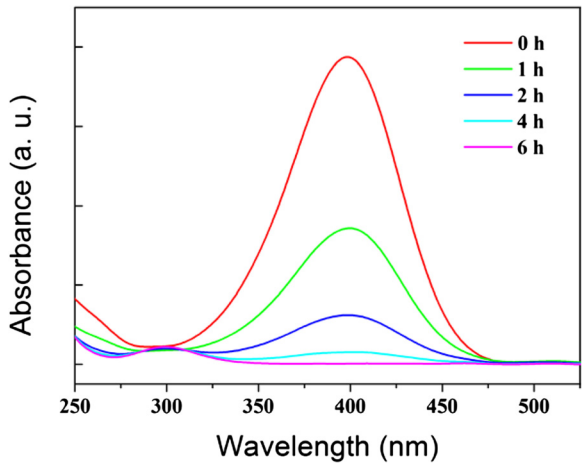

Fig. 5 Time-dependent UV–vis spectrum of the reaction mixture for the 4-NP reduction reaction using the porous Ni microsphere as a catalyst

Additional file

Additional file 1: Figure S1. Data curves of N_2 adsorption-desorption isotherms and pore size distributions. N_2 adsorption-desorption isotherms (A) and pore size distributions (B) for polymer template, Polymer/EDA, Ni precursor, NiO and Ni microspheres. (PDF 168 kb)

Abbreviations

GMA: glycidyl methacrylate; EGDMA: ethylene glycol dimethacrylate; EDA: ethylene diamine; 4-NP: 4-nitrophenol; 4-AP: 4-aminophenol; XRD: X-ray diffraction; SEM: scanning electron microscope; BET: Brunauer-Emmett-Teller; BJH: Barrett-Joyner-Halenda.

Competing Interests

The authors declare that they have no competing interests.

Authors' Contributions

CT, YW, and MH designed the experiment. CT and JH carried out the experiment, as well as wrote the manuscript. LZ was involved in the characterization and analysis of the data, as well as helped to prepare the manuscript. LR carried out the catalytic experiment, analyzed the data, and

helped to prepare the manuscript. JC helped to draft and correct the manuscript. All authors read and approved the final manuscript.

Acknowledgements
This work was financially supported by the grant of National Natural Science Foundation of China (21304003), Guangdong Science and Technology Program (2013A061401002), and the Shenzhen Strategic Emerging Industries Project (JCYJ20140627145346390, JCYJ20140903102140989, JCYJ20140903102042989, SGLH20131010153302024).

Received: 25 July 2015 Accepted: 21 September 2015
Published online: 05 October 2015

Reference

1. Yin Y, Alivisatos AP. Colloidal nanocrystal synthesis and the organic–inorganic interface. Nature. 2005;437(7059):664–70.
2. Neuberger T, Schopf B, Hofmann H, Hofmann M, von Rechenberg B. Superparamagnetic nanoparticles for biomedical applications: possibilities and limitations of a new drug delivery system. J Magn Magn Mater. 2005;293(1):483–96.
3. Crooks RM, Zhao MQ, Sun L, Chechik V, Yeung LK. Dendrimer-encapsulated metal nanoparticles: Synthesis, characterization, and applications to catalysis. Accounts Chem Res. 2001;34(3):181–90.
4. Moreno-Manas M, Pleixats R. Formation of carbon-carbon bonds under catalysis by transition-metal nanoparticles. Accounts Chem Res. 2003;36(8):638–43.
5. Budarin VL, Clark JH, Luque R, Macquarrie DJ, White RJ. Palladium nanoparticles on polysaccharide-derived mesoporous materials and their catalytic performance in C-C coupling reactions. Green Chem. 2008;10(4):382–7.
6. Winnischofer H, Rocha TCR, Nunes WC, Socolovsky LM, Knobel M, Zanchet D. Chemical synthesis and structural characterization of highly disordered ni colloidal nanoparticles. ACS Nano. 2008;2(6):1313–9.
7. Campelo JM, Conesa TD, Gracia MJ, Jurado MJ, Luque R, Marinas JM, et al. Microwave facile preparation of highly active and dispersed SBA-12 supported metal nanoparticles. Green Chem. 2008;10(8):853–8.
8. Mitsudome T, Mikami Y, Ebata K, Mizugaki T, Jitsukawa K, Kaneda K. Copper nanoparticles on hydrotalcite as a heterogeneous catalyst for oxidant-free dehydrogenation of alcohols. Chem Commun. 2008;39:4804–6.
9. Roucoux A, Schulz J, Patin H. Reduced transition metal colloids: a novel family of reusable catalysts? Chem Rev. 2002;102(10):3757–78.
10. El-Sayed MA. Some interesting properties of metals confined in time and nanometer space of different shapes. Accounts Chem Res. 2001;34(4):257–64.
11. Favier I, Madec D, Teuma E, Gomez M. Palladium nanoparticles applied in organic synthesis as catalytic precursors. Curr Org Chem. 2011;15(18):3127–74.
12. Zahmakiran M, Ozkar S. Metal nanoparticles in liquid phase catalysis; from recent advances to future goals. Nanoscale. 2011;3(9):3462–81.
13. Bell AT. The impact of nanoscience on heterogeneous catalysis. Science. 2003;299(5613):1688–91.
14. Ma TY, Yuan ZY. Metal phosphonate hybrid mesostructures: environmentally friendly multifunctional materials for clean energy and other applications. ChemSusChem. 2011;4(10):1407–19.
15. Studer M, Blaser HU, Exner C. Enantioselective hydrogenation using heterogeneous modified catalysts: an update. Adv Synth Catal. 2003;345(1–2):45–65.
16. Astruc D, Lu F, Aranzaes JR. Nanoparticles as recyclable catalysts: the frontier between homogeneous and heterogeneous catalysis. Angew Chem-Int Edit. 2005;44(48):7852–72.
17. Liang HP, Zhang HM, Hu JS, Guo YG, Wan LJ, Bai CL. Pt hollow nanospheres: facile synthesis and enhanced electrocatalysts. Angew Chem-Int Edit. 2004;43(12):1540–3.
18. Ewers TD, Sra AK, Norris BC, Cable RE, Cheng CH, Shantz DF, et al. Spontaneous hierarchical assembly of rhodium nanoparticles into spherical aggregates and superlattices. Chem Mat. 2005;17(3):514–20.
19. Zhao MQ, Sun L, Crooks RM. Preparation of Cu nanoclusters within dendrimer templates. J Am Chem Soc. 1998;120(19):4877–8.
20. Zhu CZ, Han L, Hu P, Dong SJ. In situ loading of well-dispersed gold nanoparticles on two-dimensional graphene oxide/SiO2 composite nanosheets and their catalytic properties. Nanoscale. 2012;4(5):1641–6.
21. Vidoni O, Philippot K, Amiens C, Chaudret B, Balmes O, Malm JO, et al. Novel, spongelike ruthenium particles of controllable size stabilized only by organic solvents. Angew Chem-Int Edit. 1999;38(24):3736–8.
22. Ould-Ely T, Amiens C, Chaudret B, Snoeck E, Verelst M, Respaud M, et al. Synthesis of nickel nanoparticles: influence of aggregation induced by modification of poly(vinylpyrrolidone) chain length on their magnetic properties. Chem Mat. 1999;11(3):526–9.
23. Sapkal SB, Shelke KF, Shingate BB, Shingare MS. Nickel nanoparticle-catalyzed facile and efficient one-pot synthesis of polyhydroquinoline derivatives via Hantzsch condensation under solvent-free conditions. Tetrahedron Lett. 2009;50(15):1754–6.
24. Liu SX, Yang YH, Zhen XL, Li JZ, He HM, Feng J, et al. Enhanced reduction of C-N multiple bonds using sodium borohydride and an amorphous nickel catalyst. Org Biomol Chem. 2012;10(3):663–70.
25. Li TL, Zhang WN, Lee RZ, Zhong QX. Nickel-boron alloy catalysts reduce the formation of trans fatty acids in hydrogenated soybean oil. Food Chem. 2009;114(2):447–52.
26. Saxena A, Kumar A, Mozumdar S. Ni-nanoparticles: an efficient green catalyst for chemo-selective oxidative coupling of thiols. J Mol Catal A-Chem. 2007;269(1–2):35–40.
27. Chen GX, Zhao YH, Lv D, Zhao TJ, Zhu Y, Sun YA. Kinetically controlled synthesis of nickel tetrahedron nanocrystals for high performance catalytic hydrogenation. RSC Adv. 2013;3(16):5314–7.
28. Yang JL, Duan GT, Cai WP. Controllable fabrication and tunable magnetism of nickel nanostructured ordered porous arrays. J Phys Chem C. 2009;113(10):3973–7.
29. Tang SC, Zheng Z, Vongehr S, Meng XK. Facile and rapid synthesis of nickel nanowires and their magnetic properties. J Nanopart Res. 2011;13(12):7085–94.
30. Wang JJ, Pang H, Yin JZ, Guan LN, Lu QY, Gao F. Controlled fabrication and property studies of nickel hydroxide and NiO nanostructures. Crystengcomm. 2010;12(5):1404–9.
31. Puntes VF, Krishnan KM, Alivisatos AP. Colloidal nanocrystal shape and size control: the case of cobalt. Science. 2001;291(5511):2115–7.
32. Xia YN, Xiong YJ, Lim B, Skrabalak SE. Shape-controlled synthesis of metal nanocrystals: simple chemistry meets complex physics? Angew Chem-Int Edit. 2009;48(1):60–103.
33. Kimura T, Yamauchi Y. Electron microscopic study on aerosol-assisted synthesis of aluminum organophosphonates using flexible colloidal PS-b-PEO templates. Langmuir. 2012;28(35):12901–8.
34. Ma TY, Yuan ZY. Periodic mesoporous titanium phosphonate spheres for high dispersion of CuO nanoparticles. Dalton Trans. 2010;39(40):9570–8.
35. Whitesides GM, Grzybowski B. Self-assembly at all scales. Science. 2002;295(5564):2418–21.
36. Banerjee S, Santhanam A, Dhathathreyan A, Rao PM. Synthesis of ordered hexagonal mesostructured nickel oxide. Langmuir. 2003;19(13):5522–5.
37. Wu MS, Yang CH, Wang MJ. Morphological and structural studies of nanoporous nickel oxide films fabricated by anodic electrochemical deposition techniques. Electrochim Acta. 2008;54(2):155–61.
38. Zhu QW, Zhang YH, Wang JJ, Zhou FS, Chu PK. Facile synthesis of hollow and porous nickel microspheres by low temperature molecular self-assembly. Solid State Sci. 2011;13(2):438–43.
39. Bartlett PN, Ghanem MA, El Hallag IS, de Groot P, Zhukov A. Electrochemical deposition of macroporous magnetic networks using colloidal templates. J Mater Chem. 2003;13(10):2596–602.
40. Zhu YP, Liu YL, Ren TZ, Yuan ZY. Mesoporous nickel phosphate/phosphonate hybrid microspheres with excellent performance for adsorption and catalysis. RSC Adv. 2014;4(31):16018–21.
41. Bakker ML, Young DJ, Wainwright MS. Selective leaching of NiAl3 and Ni2Al3 intermetallics to form Raney nickels. J Mater Sci. 1988;23(11):3921–6.
42. Hoffer BW, Crezee E, Devred F, Mooijman PRM, Sloof WG, Kooyman P, et al. The role of the active phase of Raney-type Ni catalysts in the selective hydrogenation of D-glucose to D-sorbitol. Appl Catal A-Gen. 2003;253(2):437–52.
43. Dominguez X, Lopez IC, Franco R. Simple preparation of a very active Raney nickel catalyst. J Org Chem. 1961;26(5):1625.
44. Hochard F, Jobic H, Massardier J, Renouprez AJ. Gas phase hydrogenation of acetonitrile on Raney nickel catalysts: reactive hydrogen. J Mol Catal A-Chem. 1995;95(2):165–72.

45. Smith AJ, Trimm DL. The preparation of skeletal catalysts. Annual Review of Materials Research. Annual Review of Materials Research. Palo Alto: Annual Reviews; 2005. p. 127–42.
46. Fow KL, Ganapathi M, Stassen I, Fransaer J, Binnemans K, De Vos DE. Highly active gauze-supported skeletal nickel catalysts. Chem Commun. 2013;49(76):8498–500.
47. Fow KL, Ganapathi M, Stassen I, Binnemans K, Fransaer J, De Vos DE. Catalytically active gauze-supported skeletal nickel prepared from Ni-Zn alloys electrodeposited from an acetamide-dimethyl sulfone eutectic mixture. Catal Today. 2015;246:191–7.
48. Goetsch DA, Schmidt LD. Microsecond catalytic partial oxidation of alkanes. Science. 1996;271(5255):1560–2.
49. Xiong JF, Shen H, Mao JX, Qin XT, Xiao P, Wang XZ, et al. Porous hierarchical nickel nanostructures and their application as a magnetically separable catalyst. J Mater Chem. 2012;22(24):11927–32.
50. Yong W, Qingshan Z, Huigang Z. Fabrication and magnetic properties of hierarchical porous hollow microspheres. J Mater Chem. 2006;16(13):1212–4.
51. He J, Yang CL, Xiong XH, Jiang BW. Preparation and characterization of monodisperse porous silica microspheres with controllable morphology and structure. J Polym Sci Pol Chem. 2012;50(14):2889–97.
52. Wang Y, He J, Chen JW, Ren LB, Jiang BW, Zhao J. Synthesis of monodisperse, hierarchically mesoporous, silica microspheres embedded with magnetic nanoparticles. ACS Appl Mater Interfaces. 2012;4(5):2735–42.
53. Ren LB, Teng C, Zhu LL, He J, Wang Y, Zuo XB, et al. Preparation of uniform magnetic recoverable catalyst microspheres with hierarchically mesoporous structure by using porous polymer microsphere template. Nanoscale Res Lett. 2014;9:1–8.
54. He J, Chen JW, Ren LB, Wang Y, Teng C, Hong M, et al. Fabrication of monodisperse porous zirconia microspheres and their phosphorylation for Friedel-Crafts alkylation of indoles. ACS Appl Mater Interfaces. 2014;6(4):2718–25.
55. Cheng J, Wang Y, Teng C, Shang Y, Ren L, Jiang B. Preparation and characterization of monodisperse, micrometer-sized, hierarchically porous carbon spheres as catalyst support. Chem Eng J. 2014;242:285–93.
56. Bao J, Liang Y, Xu Z, Si L. Facile synthesis of hollow nickel submicrometer spheres. Adv Mater. 2003;15(21):1832–5.
57. Chen D-H, Hsieh C-H. Synthesis of nickel nanoparticles in aqueous cationic surfactant solutions. J Mater Chem. 2002;12(8):2412–5.
58. Hwang J-H, Dravid VP, Teng MH, Host JJ, Elliott BR, Johnson DL, et al. Magnetic properties of graphically encapsulated nickel nanocrystals. J Mater Res. 1997;12(04):1076–82.